tvst

Article

Mitochondrial Transfer of the Mutant Human *ND6T14484C* Gene Causes Visual Loss and Optic Neuropathy

Hong Yu[1], David W. Sant[2], Gaofeng Wang[3], and John Guy[1]

[1] Bascom Palmer Eye Institute, University of Miami, Miller School of Medicine, Miami, FL, United States
[2] Department of Biomedical Informatics, University of Utah, Salt Lake City, UT, United States
[3] John P. Hussman Institute for Human Genomics, Dr. John T. MacDonald Foundation Department of Human Genetics, University of Miami, Miller School of Medicine, Miami, FL, United States

Correspondence: John Guy, 1638 NW 10th Ave, Mcknight 404, Miami, FL 33136, USA. e-mail: jguy@med.miami.edu, hyu3@med.miami.edu

Received: May 7, 2020
Accepted: September 1, 2020
Published: October 1, 2020

Keywords: LHON; animal model; MTS-AAV; gene delivery

Citation: Yu H, Sant DW, Wang G, Guy J. Mitochondrial transfer of the mutant human *ND6T14484C* gene causes visual loss and optic neuropathy. Trans Vis Sci Tech. 2020;9(11):1, https://doi.org/10.1167/tvst.9.11.1

Purpose: To evaluate the long-term effects of mitochondrial gene transfer of mutant human NADH ubiquinone oxidoreductase subunit VI (*hND6T14484C*) in the mouse eye.

Methods: Adult mice were injected intravitreally with mitochondrial-targeted adeno-associated virus carrying either *hND6T14484C* or mitochondrial encoded *mCherry*. The delivery and expression of the interest gene were detected by polymerase chain reaction (PCR), quantitative PCR (qPCR), and immunostaining. The pathologic effects of the mutant gene in live mice were assessed with RNA-seq, serial spectral domain optical coherence tomography (SD-OCT), and pattern electroretinogram (PERG).

Results: Delivered *hND6* was found 30-fold greater than endogenous mouse *ND6* in microdissected retinal ganglion cells of *hND6*-injected mice. Compared to controls injected with *mCherry*, PERG amplitude of *hND6* mice dropped significantly at 3 ($P = 0.0023$), 6 ($P = 0.0058$), and 15 ($P = 0.031$) months after injection. SD-OCT revealed swelling of the optic nerve head followed by the progressive retinal and optic nerve atrophy in *hND6* mice. Furthermore, RNA-seq data showed a change in 381 transcripts' expression in these mice compared to *mCherry* mice. Postmortem analysis showed *hND6* mice had marked atrophy of the entire optic nerve, from the globe to the optic chiasm, and a significant loss of retinal ganglion cells compared to age-matched control mice ($P = 1.7E\text{-}9$).

Conclusions: Delivered *hND6T14484C* induces visual loss and optic neuropathy in mice, the hallmarks of human Leber's hereditary optic neuropathy (LHON).

Translational Relevance: Results from this study will help establish a novel strategy not only to generate an LHON animal model but also to provide a potential to treat this or any other mitochondrial diseases.

Introduction

Mitochondrial dysfunction causes a broad spectrum of human diseases that primarily affect the eye and nervous system. Treatment for these devastating disorders is inadequate in large part due to the absence of relevant animal models to demonstrate preclinical efficacy to the US Food and Drug Administration necessary to obtain an investigational new drug permit. The most common primary mitochondrial genetic disease is Leber's hereditary optic neuropathy (LHON),[1,2] which was associated with a mitochondrial DNA (mtDNA) point mutation in 1988.[3] Currently, 37 different causative point mutations have been described,[4] among them three primary mutations that affect different subunits of respiratory complex I, *ND1G3460A*,[5,6] *ND4 G11778A*,[3] and *ND6T14484C*,[7,8] accounting for about 95% of LHON cases. Patients develop acute or subacute painless loss of central vision in both eyes, although one eye may be affected 6 to 8 weeks before vision loss in the second eye.[4,9] Most symptomatic patients are male. Most LHON cases are homoplasmic (all mtDNA molecules

contain the mutation) for any of these mutations; still, heteroplasmic cases (a mixture of mutant and wild-type mtDNA) also exist, more frequently with either *ND1G3460A* or *ND6T14484C* mutations.[10,11] There is no discernible phenotypic difference between the heteroplasmic and homoplasmic patients.[4] Common to all cases of LHON is a progressive degeneration of retinal ganglion cells (RGCs) and axons of the optic nerve.

Animal models bearing the same mtDNA mutations as found in patients with LHON are needed to investigate the pathogenesis and test potential therapeutic strategies. However, generating genetic animal models of LHON or any other mitochondrial diseases is challenging because of difficulties in direct delivery and incorporation of genetic material within mtDNA. Lin et al.[12] generated a mouse model bearing the equivalent of the human *ND6G14600A* P25L mutation that causes human Leigh syndrome.[13] While their transgenic mice had a mild axonal loss in the optic nerve, visual function was normal. In previous studies, we generated an LHON animal model by allotopically expressing human ND4G11778A R340H. With visual and RGC loss, our mouse model had the hallmarks of human LHON.[14–16] The Corral-Debrinski group used a similar strategy to develop a rodent model by electroporating allotopic mutant *ND4*.[17,18] We, two groups, rescued rodent models with injections of adeno-associated viruses (AAVs) containing wild-type human *ND4*. This work formed the basis for launching gene therapy trials designed to test the safety and therapeutic effects of the allotopically expressed human ND4 on patients blinded from the *ND4G11778A* mutation.[19–24] Currently, there are no gene therapy trials for the other LHON genotypes caused by *ND1* or *ND6* mutations.

Our laboratory has pioneered a novel approach to redirect the AAV virion to mitochondria by addition of a mitochondrial targeting sequence (MTS) to the capsid VP2 (MTS-AAV).[25,26] Using the MTS-AAV, we introduced human *ND4G11778A* gene into mouse zygotes and generated a bona fide LHON mitomice bearing human *ND4G11778A*. The translated human ND4 protein assembled into host respiratory complexes decreased respiratory chain function and increased oxidative stress. The *ND4* mitomice recapitulated the progressive RGC loss and optic nerve degeneration observed in patients with LHON.[27] Here, we use the MTS-AAV to deliver human *ND6T14484C* into the mouse visual system by intravitreal injection to generate a mouse model of visual and RGC loss with the hallmarks of human LHON.

Methods

Plasmids and AAVs

scHSPCSB-hND6T14484C-mCherry was constructed as previously described.[25,27] In brief, human *ND6T14484C* gene fused in frame with an *HA* tag was cloned into a self-complementary AAV (scAAV) backbone under the control of mitochondrial heavy strand promoter, including three upstream conserved sequence blocks (*HSPCSB*). Then, mitochondrial-encoded *Cherry* (*mCherry*) containing a kozak sequence was put downstream of *ND6T14484CHA* with a stop codon between two genes (scHSPCSB-ND6 T14484CmCherry). Meanwhile, *mCherry* was cloned in the same scAAV backbone and used as a control (scHSPCSB-mCherry). The resultant plasmids were packaged into recombinant MTS-AAVs.

Animals

All animal procedures were performed following the National Institutes of Health Guide for Care and Use of Laboratory Animals and the ARVO Statement for the Use of Animals in Ophthalmic and Vision Research. Intravitreal injections of 1 µL recombinant MTS-AAVs were performed on 3-month-old DBA/1j mice as previously described.[14]

RNA-Seq

RNA-seq was performed on the optic nerve of mice injected with either mutant *hND6* or *mCherry* AAVs (three mice in each group). Total RNA was extracted from the optic nerve of each mouse using the RNeasy Mini Kit (Qiagen, Hilden, Germany). Sequencing was carried out at the Sequencing Core of John P. Hussman Institute of Human Genomics at the University of Miami using the TruSeq Stranded Total RNA Library Prep Kit (Illumina, San Diego, CA).

Data were analyzed using a previously published pipeline.[28] Briefly, after quality control, reads were aligned to the mouse transcriptome (GRCm38; Ensembl.org; in the public domain) and quantified using the STAR aligner.[29] Statistical significances between the two groups were determined using DESeq2 with a cutoff-adjusted *P* value of 0.05.[30]

Pattern Electroretinography and Optical Coherence Tomography

Pattern electroretinogram (PERG) was performed as previously described.[31,32] Averaged PERGs were automatically analyzed to evaluate the significant positive and negative waves by Sigma Plot (Systat Software, San Jose, CA). Retinal images were visualized using *in vivo* spectral domain optical coherence tomography (SD-OCT) (Bioptigen, Durham, NC). Then the average thickness of RGC+IPL of 100 scans covering the whole retina was calculated using a semiautomated custom software written with MATLAB software (MathWorks, Natick, MA).

Laser Microdissection and Polymerase Chain Reaction

The injected mouse retinas were fixed overnight at 4°C in 4% paraformaldehyde (PFA)/phosphate-buffered saline (PBS) and equilibrated in 30% sucrose/PBS overnight at 4°C. After embedding into Optimal Cutting Temperature Compound (OCT), the retinas were cut into 8-µm sections and placed onto the director slides (Expression Pathology, Rockville, MD). Laser capture microdissection was performed using a Leica LMD6500. DNA was extracted from cells in the RGC and inner and outer nuclear layers using the DNeasy blood and tissue kit (Qiagen).

Polymerase chain reaction (PCR) primers: 5′-AATTTCCACCAAACCCCCCC-3′, 5′-TCCCG AATCAACCCTGACCC 3′.

Quantitative PCR (qPCR) primers: *hND6:* 5′-TGATGGGGTGGTGGTTGTGG-3′; 5′-AAGCCC CCGCACCAATAGG-3′; *mND6:* 5′-TTGGTTGGT TGTCTTGG-3′; 5′-CACCAAACCCTAAAACC-3′.

Immunohistochemistry

Mice were perfused transcardially with PBS followed by 4% PFA in PBS. For whole-mount retinal staining, mice were injected intravitreally with 1 µL MitoTracker Deep Red (500 nM) 20 minutes before the perfusion. Eyeballs were enucleated and fixed in 4% PFA for 15 minutes. The retina was dissected out, put in 30% sucrose overnight at 4°C, and used for staining. The following antibodies were used: anti-HA (1:500; Abcam, Cambridge, MA), anti-RBPMS (1:200; PhosphoSolutions, Aurora, CO), anti-active CASPASE3 (1:200; Abcam), anti-rabbit IgG 546 (1:600; Invitrogen, Carlsbad, CA), anti-mouse IgG 488 (1:600; Invitrogen), and anti–guinea pig 647 (1:600; Invitrogen). Imagines were taken with a Leica TCS SP5 confocal microscope.

Respiratory Chain Function

The optic nerves were dissected out right after the euthanasia. Assays of complex I activity were performed in triplicate using complex I enzyme activity microplate assay kits (Abcam). The rate of adenosine triphosphate (ATP) synthesis was measured in triplicate by chemiluminescence with a modified luciferin-luciferase assay as described previously.[25,27] Synthesized ATP was detected in real time with an Optocom I luminometer (MGM Instruments, Hamden, CT). The protein concentration of each suspension was quantitated using the protein assay kit (Bio-Rad, Hercules, CA).

Statistical Analysis

Statistical analyses were performed using the GraphPad Prism6 software (GraphPad Software, La Jolla, CA). Two groups were compared using two-tailed *t* tests, and multiple groups were compared using one-way analysis of variance, and Tukey's multiple comparisons test, with P values of <0.05 considered significant. Values were expressed as means ± SDs.

Results

Human *ND6T14484C* Was Delivered into Cells of the Ganglion Cell Layer of the Mice

Human *ND6T14484C* linked to an *HA* tag and *mCherry* (*hND6T14484C*) was cloned into an AAV backbone (Fig. 1A). The same AAV backbone carrying only *mCherry* was used as a control. All resultant constructs were packaged into MTS-AAVs. In one group of 10 animals (unilateral injection group), mice were injected with *hND6T14484C* into one eye and *mCherry* into the fellow eye. In another group of 26 animals (bilateral injection group), mice were randomly divided into two groups and injected with either *hND6T14484C* or *mCherry* in both eyes (Supplementary Table S1). To reflect the male predominance of LHON, all mice were male. Ten days after intravitreal injections, qPCR performed on microdissected cells revealed that the ratio of *hND6* level to that of endogenous mouse *ND6* was 31 in cells of the ganglion cell layer (GCL). This ratio, however, was only 1 in cells of the inner nuclear layer (INL) and 6 in cells of the outer nuclear layer (ONL) in *hND6T14484C*-injected mice (Fig. 1B). These findings were consistent with previous reports that AAV2 efficiently infects RGCs after intravitreal injection of adult rodent eyes.[33–35] No *hND6* was detected in any retinal layer of *mCherry*-injected

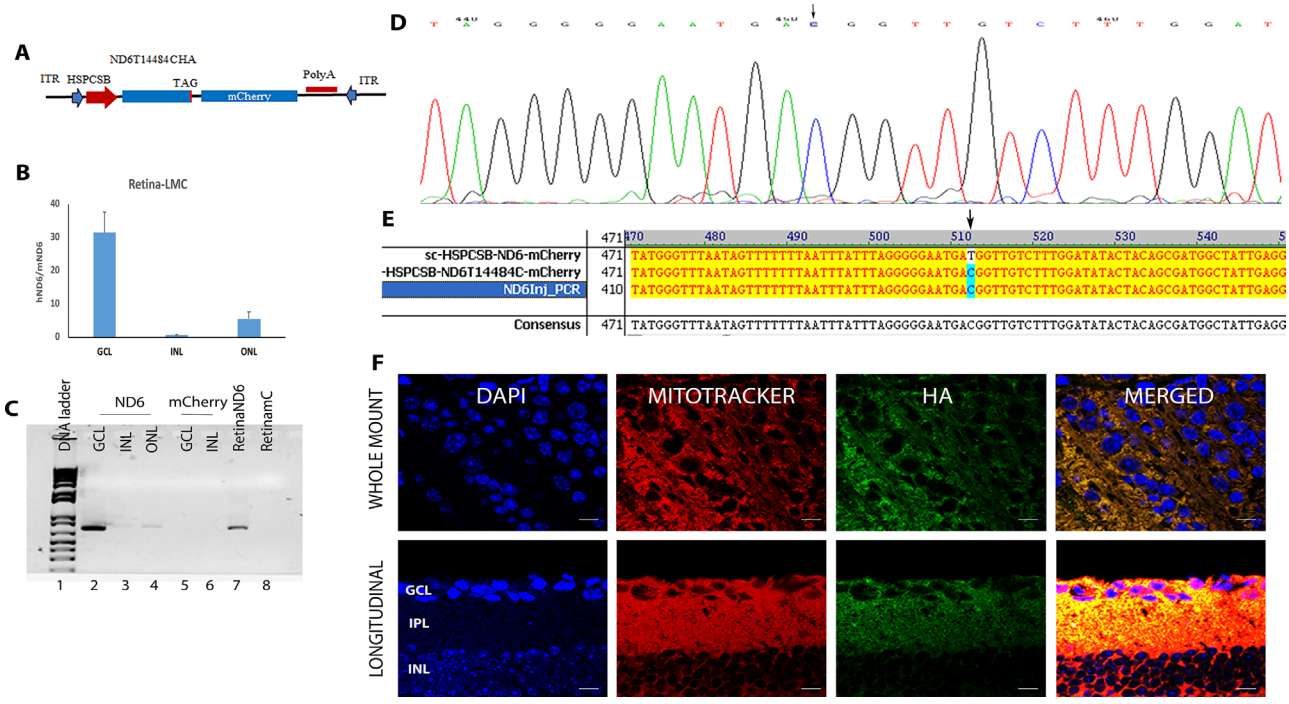

Figure 1. Delivery and expression of *hND6T14484C* in the retinal ganglion cells of the injected mice. (A) Schematic of an AAV construct where the *hND6T14484C* gene fused with the *HA* epitope tag was cloned into a self-complementary AAV backbone, under the control of the mitochondrial heavy strand promoter, including three upstream conserved sequence blocks (*HSPCSB*) of the D-loop responsible for replication. A fluorescence marker, mitochondrial encoded *mCherry*, was cloned downstream of the mutant gene with a stop codon TAG in between. (B) qPCR on microdissected cells showed that *hND6* was 31 times of endogenous mouse *ND6* in the retinal GCL, 1 time in the INL, and 6 times in the ONL. (C) Using the forward primer targeted to *HSPCSB* and reverse primer targeted to human *ND6*, the PCR showed bands with expected size in the whole retina (RetinaND6, lane 7) and microdissected cells from the retinal GCL (lane 2), INL (lane 3), and ONL (lane 4) of mutant *hND6*-injected mice but not in any layer or whole retina (RetinamC) of the control mouse (lanes 5, 6, 8). (D) Sequencing confirmed the amplified band was *hND6T14484C* (*arrow*, the *bluish wave*). (E) PCR sequence aligned to plasmids carrying wild-type *hND6* and *hND6T14484C* respectively further confirmed that the PCR product was the mutant *hND6T14484C* (*arrow*). (F) Representative immunostaining of the whole mount and longitudinal section of a retina showed that HA was expressed in cells in the RGC layer and colocalized with a MitoTracker Deep Red. *Scale bars*: 10 µm.

mice. PCR using primers targeting the *hND6T14484C* construct showed bands of the expected size in the whole retina (Fig. 1C, lane 7) and microdissected cells from the GCL, INL, and ONL in mutant *hND6*-injected mice (Fig. 1C, lanes 2–4). No bands were found in the whole retina or microdissected cells from the GCL and INL in control mice (Fig. 1C, lanes 5, 6, and 8). Sequencing and alignment to the mutant and wild-type *hND6* confirmed that the PCR product was *hND6T14484C* (Figs. 1D, 1E). Immunohistochemistry showed that HA staining was colocalized with MitoTracker Deep Red. The HA-expressing cells were located only in the ganglion cell layer of *hND6T14484C*-injected mouse retinas (Fig. 1F).

Mutant *hND6* Causes Retinal Degeneration

SD-OCT can be used to visualize layers of the retina in live animals. As the mouse retinal ganglion cell layer is too thin for SD-OCT dependable resolution, we measured the thickness of the RGC and the inner plexiform layers (RGC + IPL). We found swelling of the optic nerve head and the adjacent RGC + IPL, compatible with early human LHON, began 1 month after intravitreal injections of *hND6T14484C*. The swelling persisted up to 4 months after injection. These findings are also compatible with early human LHON. Later, we detected progressive thinning of the RGC + IPL (Fig. 2A), as seen in later atrophic stages of human LHON. Semiautomated quantification showed that the thickness of RGC + IPL increased significantly 1 month after injection (85.5 ± 10.8 µm vs. 72.14 ± 2.0 µm at baseline, $P < 0.05$), then dropped at 4 months (79.7 ± 21.6 µm) and continually dropped to 65.0 ± 8.1 µm at 8 months ($P < 0.001$) and 62.3 ± 8.4 µm at 14 months ($P < 0.01$) after injection (Fig. 2C). We did not find any qualitative change in RGC + IPL thickness from baseline

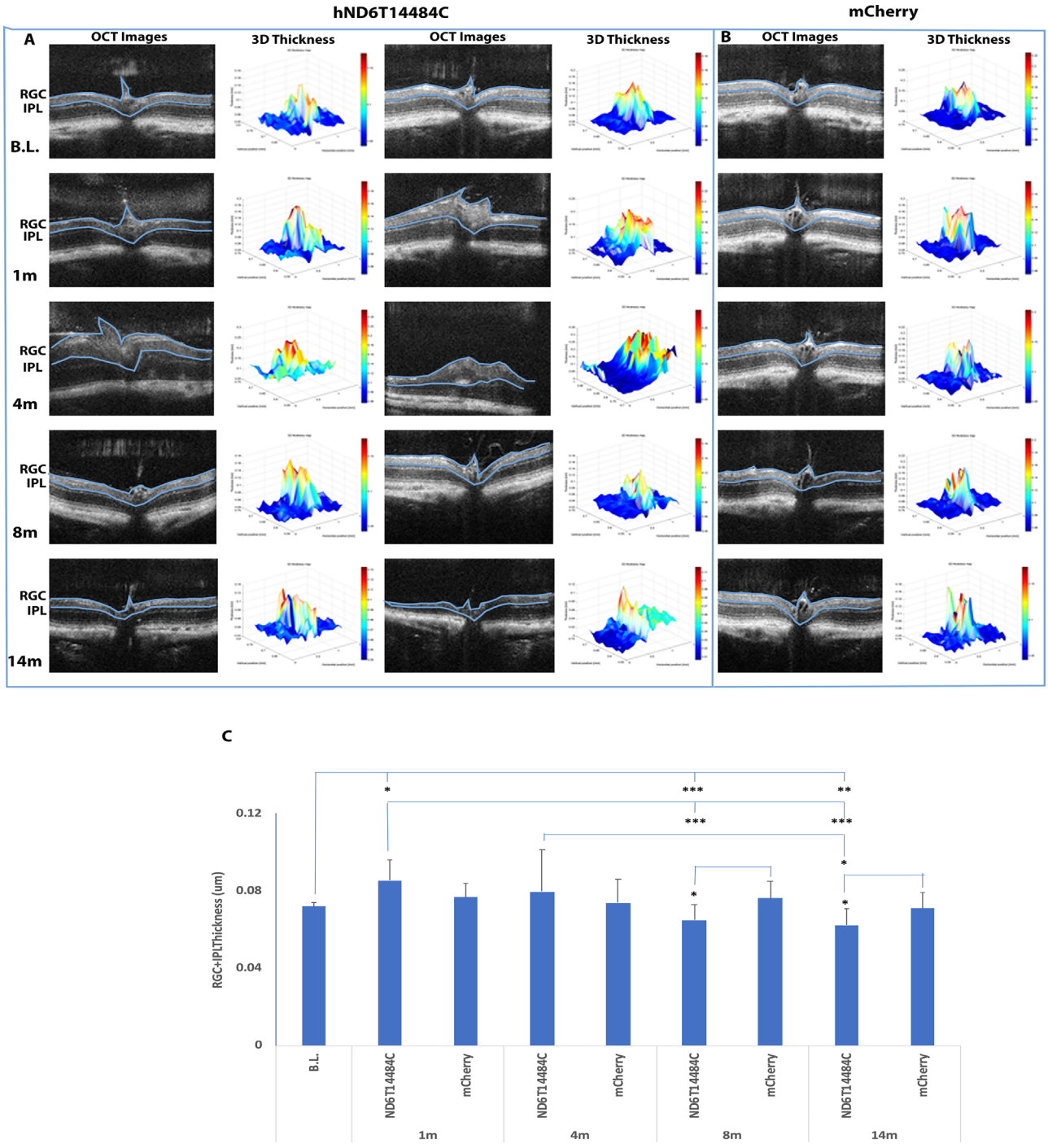

Figure 2. *hND6T14484C* causes retinal degeneration. Representative SD-OCT images and the corresponding three-dimensional (3D) thickness of RGC-IPL maps of two mice injected with mutant *ND6* (A) and one mouse injected with *mCherry* (B). Each SD-OCT image (OCT image) represents one scan of a retina where the RGC+IPL layers were highlighted in between two *blue lines*, and the corresponding 3D map (3D Thickness of RGC + IPL) was generated from 100 OCT images covering one whole retina using a semiautomated custom software developed from MATLAB software (MathWorks). (A) In mutant *ND6*-injected mice, optic nerve head swelling was detected as early as 1 month (1m) after the injection, and the swelling could persist up to 4 months (4m) after the injection followed by a progressive loss of the RGC + IPL layers. (B) No abnormality was seen in the *mCherry*-injected control mice during the entire experimental period. (C) Quantification of the thickness of the RGC + IPL layers. Semiautomatic quantification ($n = 10$ in each group) showed a significant increase in the thickness of RGC + IPL layers followed by a progressive decrease of this thickness in mutant hND6-injected mice. The difference in the thickness of RGC + IPL between baseline (B.L.) and 1 month (1m), 8 months (8m), and 14 months (14m) after injection was significant ($P < 0.05$, 0.001, and 0.01, respectively). The differences in the thickness between 1m and 8m or 14m were also significant ($P < 0.001$). Meanwhile, compared to age-matched control mice, mice injected with mutant hND6 showed a significant thinning of the RGC + IPL layers at 8m ($P < 0.05$) and 14m ($P < 0.05$).

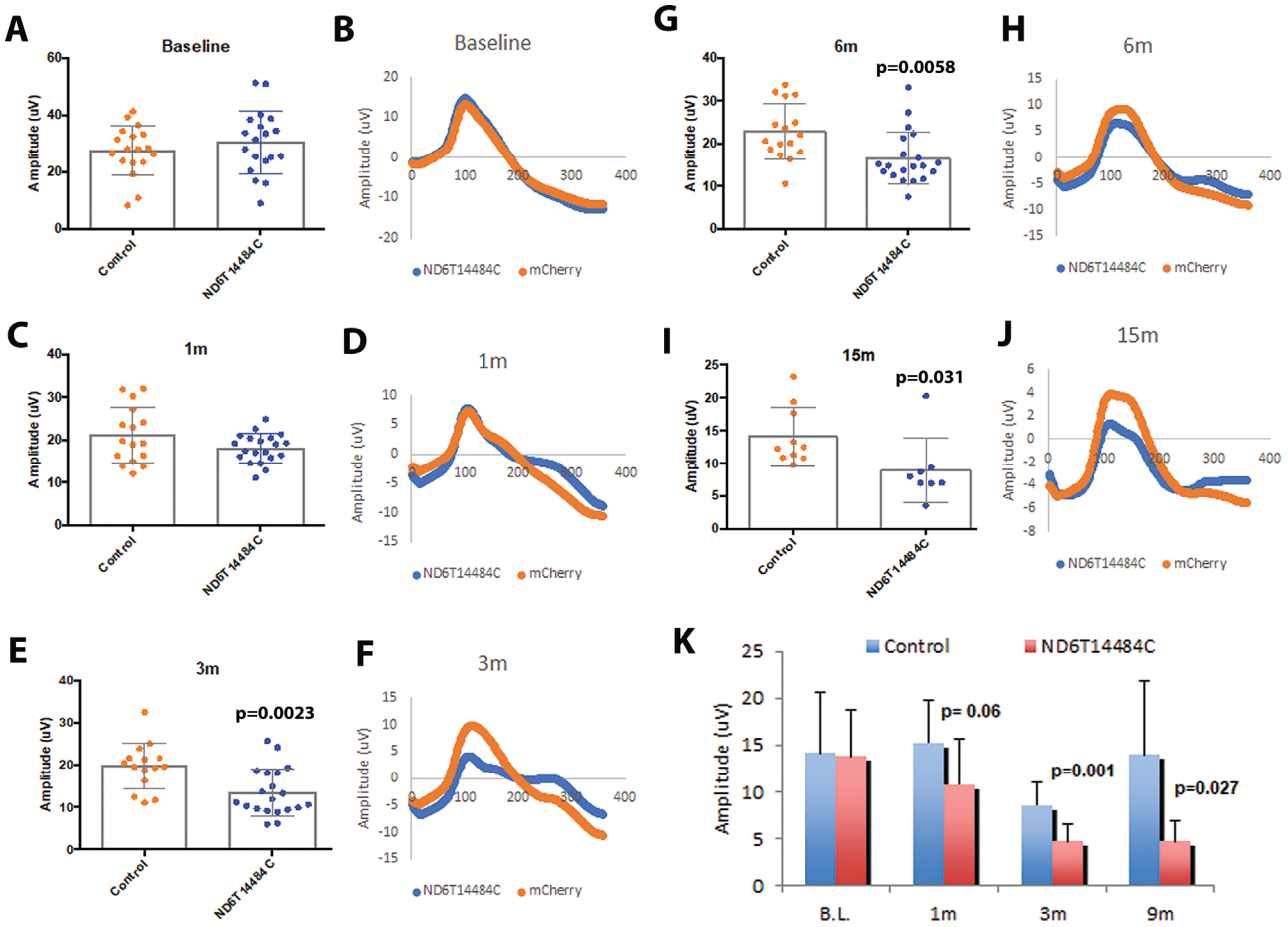

Figure 3. Vision loss is induced by *hND6T14484C*. Scatterplots of PERG amplitudes and averaged waveforms of all mice tested in each group showed no significant difference between the mice bilaterally injected with *hND6T1448C* ($n = 20$ eyes) and the mice bilaterally injected with *mCherry* ($n = 20$ eyes) at the baseline (A, B) and 1 month (1m) after injection (C, D). However, the difference became statistically significant at 3 months (3m, $P = 0.0023$, E, F), 6 months (6m, $P = 0.0058$, G, H), and 15 months (15m, $P = 0.031$, I, J) after injection. (K) A bar graph ($n = 10$) showed a gradual decrease in PERG amplitude in eyes unilaterally injected with *hND6T14484C* compared to eyes unilaterally injected with *mCherry* (control). The decrease became significantly at 3 months (3m, $P = 0.001$) and 9 months (9m, $P = 0.027$) after injection.

to 1, 4, 8, and 14 months after the injection of *mCherry* (Figs. 2B, 2C). Meanwhile, compared to age-matched control mice (mCherry), mice injected with mutant *hND6* (ND6T14484C) showed significant reductions in RGC + IPL thickness at 8 months ($P < 0.05$) and 14 months ($P < 0.05$) after the injection (Fig. 2C).

Expression of Mutant *hND6* Causes Visual Loss

Given that RGC appears to be the vulnerable cell type in patients with LHON mutations, we used PERGs to determine whether *hND6T14484C* induces RGC dysfunction in mice. The PERG is a measure of visual and RGC function. For mice that had bilateral injections, we did not find statistically significant differences in PERG amplitude between the two groups of mice before intravitreal injections (Figs. 3A, 3B) and at 1 month after injection (Figs. 3C, 3D). However, we found a statistically significant decrease in the PERG amplitude at 3 months after the injection of mutant *hND6* relative to the age-matched control mice injected with *mCherry* ($P = 0.0023$; Figs. 3E, 3F). This decrement persisted at 6 months ($P = 0.0058$; Figs. 3G, 3H) and 15 months ($P = 0.031$) after the *hND6T14484C* injection (Figs. 3I, 3J). Consistently, mice with unilateral injections showed a decrease in PERG amplitude in the eye injected with mutant *hND6* compared to the eye injected with *mCherry*. The decrease became statistically significant at 3 months ($P = 0.001$) and 9 months ($P = 0.027$) after injection (Fig. 3K).

Respiratory Chain Function in *hND6T14484C*-Injected Mice

The optic nerve is highly dependent on oxidative phosphorylation and is adversely impacted by oxidative stress. Therefore, we measured complex I activity and the rate of ATP synthesis driven by malate and pyruvate in the optic nerve of the injected mice using chemiluminescence with a modified luciferin-luciferase assay. Complex I activity was not significantly reduced in the optic nerves of mutant *hND6*-injected mice (0.188 ± 0.100 OD450/min/mg, $n = 5$) compared to that of *mCherry*-injected control mice (0.248 ± 0.190 OD450/min/mg, $n = 5$, $P = 0.35$). Additionally, compared to *mCherry*-injected control mice ($n = 7$), the rate of complex I–dependent ATP synthesis was not significantly reduced in the optic nerves of mutant *hND6*-injected mice ($n = 6$, 421 ± 413 mmol ATP/min/mg protein vs. 526 ± 218 mmol ATP/min/mg protein of control mice, $P = 0.73$). Our findings in mice were consistent with previous reports that *ND6T14484C* is associated with a mild effect on complex I activity.[36]

Mutant *hND6* Causes Loss of Axons and RGCs

Postmortem analysis was performed 15 months after the injections. Gross dissections revealed marked atrophy of the entire optic nerve from behind the globe to the optic chiasm in eyes injected with *hND6T14484C* relative to eyes injected with *mCherry* (Fig. 4A). Histopathology of the retina revealed a loss of cells in the RGC layer and a thinner IPL of eyes injected with mutant *hND6* (Fig. 4B) in comparison to eyes injected with *mCherry* (Fig. 4C). Total cell counting in the RGC layer revealed that mutant *hND6*-injected mice had 28% fewer cells than age-matched control mice (4834 ± 455 cells/mm^2, vs. 6713 ± 1083 cells/mm^2, $P = 0.0209$, Fig. 4D). Consistent with cell counting, immunohistochemistry with a pan-RGC marker, RBPMS showed mice injected with mutant *hND6* had fewer RGCs (Fig. 4E) in comparison to *mCherry* control mice (Fig. 4F). Quantitative analysis revealed a 36% loss of RGCs in these mutant *hND6*-injected mice ($n = 3$, 2455 ± 773 cells/mm^2 vs. 3856 ± 743 cells/mm^2 in controls, $P = 1.7E\text{-}9$, Fig. 4G).

Mutant *hND6* Causes Apoptosis in RGCs

We found that active *Caspase 3* was abundantly expressed in the RGC layer in *hND6* bilateral injected mice 15 months after injection (Figs. 4H, 4I). These mice had 61% cells in the RGC layer positive for active CASPASE 3 staining (Fig. 4L), while the control mice only had 16% positive cells ($P = 3.74E\text{-}5$, Figs. 4L–4N). Ultrastructural analysis showed cells in the RGC layer of *hND6T14484C*-injected mice had condensation of the cytoplasm and nuclear chromatin consistent with apoptosis (Fig. 4M). Whole transcriptome sequencing (also known as RNA-seq) was performed using total RNA extracted from mouse optic nerve, the RGC's axons, at 1 month after the injection of *hND6T14484C* ($n = 3$) or *mCherry* ($n = 3$). The sequencing showed an increase in the expression of 277 transcripts and a decrease in the expression of 104 transcripts in *hND6*-injected mice in comparison to *mCherry*-injected mice (Supplementary Fig. S1). Closer inspection of the RNA-seq data shows several increased transcripts are related to the regulation of oxidative stress and apoptosis. These transcripts include *SOD1* (superoxide dismutase 1), *PRDX1* (peroxiredoxin 1), *TMBIM6* (*BAX* inhibitor 1), *PINK1* (*PTEN*-induced kinase 1), *ROMO1* (reactive oxygen species modulator 1), and so on. Their expression increased by 28% to 73% in *hND6*-injected mice compared to *mCherry*-injected mice, suggesting this increase might be due to the elevated reactive oxygen species (ROS) level in the cell (Supplementary Table S2, Supplementary Table S3). Meanwhile, using EnrichR with the list of genes upregulated in *hND6* compared to *mCherry*, an overrepresentation of genes was found in the pathway "cellular response to oxidative stress" (GO:0034599, adjusted $P = 0.0011$) and in the Gene Ontology pathway "positive regulation of intrinsic apoptotic signaling pathway" (GO: 2001244, adjusted $P = 0.00128$).[37,38] This same finding was confirmed using gene set enrichment analysis, an enrichment analysis method that uses ranking of genes rather than proportions tests (adjusted $P = 0.018$ and 0.023, Figs. 4N, 4O).[39,40] Taken together, these findings indicate that apoptosis rates were increased in the RGCs and optic nerve of *hND6T14484C*-injected mice in comparison to control mice.

Discussion

ND6T14484C is the least deleterious LHON mutation as patients with this mutation typically have a better outlook for spontaneous visual recovery than the other two primary mutations (*ND4G11778A* and *ND1G3460A*).[41–43] Mice injected with human *ND6T14484C* showed only a 14% reduction in PERG amplitude at 1 month after injection compared to age-matched control mice. This reduction is not statistically significant ($P = 0.089$), whereas mice injected with human *ND4G11778A* showed

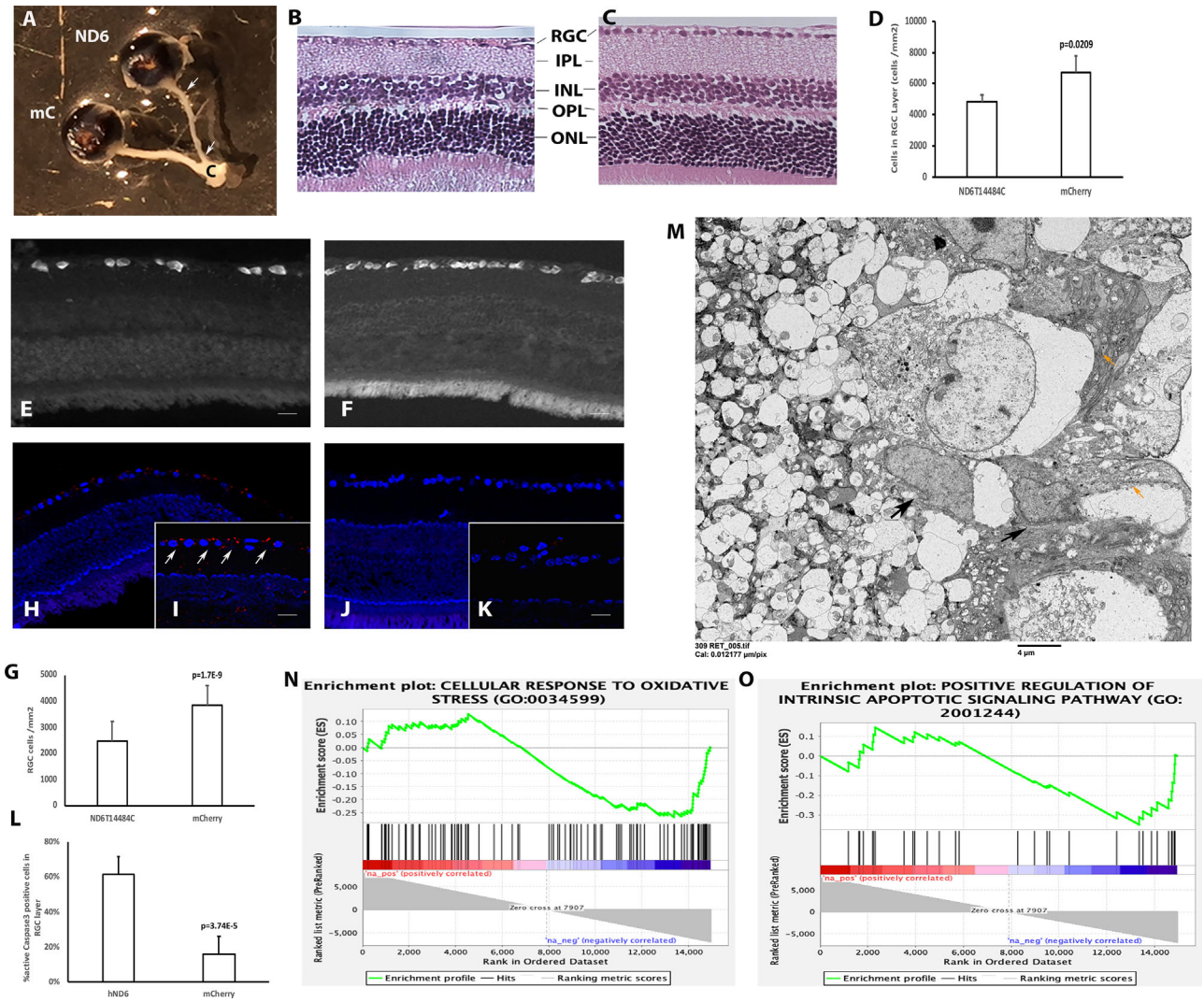

Figure 4. *hND6T14484C* causes loss of axons and RGCs. (A) Gross specimen of a unilateral injected mouse dissected 15 months after injection revealed significantly thinning of the entire optic nerve from the globe (*arrow*) to the optic chiasm (C, *arrow*) in the eye injected with *hND6T14484C* (ND6) but not in the eye injected with *mCherry* (mC). (B, C) Light microscopy images of longitudinal retinal sections performed 15 months after the injection of mutant *hND6* show that the retina has fewer cells in the RGC layer (RGC) and a thinner IPL of *hND6*-injected mice (B) compared to age-matched control mice injected with *mCherry* (C). However, no obvious difference was seen in other layers of the retina between the two mice, including INL, outer plexiform layer (OPL), and ONL. (D) Quantification ($n = 3$ in each group) shows a significant difference in cell number in the RGC layer between the two groups of mice ($P = 0.0209$). (E, F) RBPMS, a pan-RGC marker staining, showed fewer RGCs in mutant *hND6*-injected mice (E) compared to age-matched *mCherry* injected mice (F). (G) RGC quantification ($n = 3$ in each group) shows a significant difference in RGC cell number between the two groups of mice ($P = 1.7E\text{-}9$). (H–K) Active CASPASE3 staining shows more positive cells in the RGC layer (*arrows*) of mice injected with mutant *hND6* (H, I) compared to age-matched control mice (J, K). (L) Quantification ($n = 3$ in each group) showed the difference in cell number positive for active CASPASE3 was highly significant between the two groups of mice ($P = 3.74E\text{-}5$). (M) A representative transmission electron microscope image of a mouse retina shows cells in the RGC layer undergoing apoptosis 15 months after the injection of mutant *hND6* (*arrows*). (N) Gene set enrichment analysis (GSEA) enrichment plot of cellular response to oxidative stress (GO:0034599). Genes in the pathway are significantly enriched in the *hND6* samples (zero cross at 7907 in rank-ordered data set, adjusted $P = 0.018$). EnrichR analysis of this pathway was also significant (adjusted $P = 0.0011$). (O) GSEA enrichment plot of positive regulation of intrinsic apoptotic signaling pathway (GO: 2001244). Genes in the pathway are significantly enriched in the *hND6* samples (adjusted $P = 0.023$). *Scale bars*: 20 µm (B, C, E, F, H, J); 10 µm (I, K); 4 µm (M).

a significant decrease (23%) in PERG amplitude at the same time point ($P < 0.04$). The functions of the ND6 subunit remain elusive, except for its role in complex I assembly.[44,45] Structure analysis showed that mt.14484 is not a highly conserved position in ND6 protein, although it locates in the most conserved region of predicted transmembrane helix C.[42]

Mice in this study injected with *hND6T14484C* showed a mild decrement in the complex I activity and ATP synthesis that was not statistically significant. This result is strikingly similar to the *in vitro* reduction in respiration rate, where the respiration rate was lowered by about 10% to 20% in leukocytes and the lymphoblast cell line established by Epstein-Barr Virus (EBV) transformation of leukocytes isolated from patients homoplasmic for *ND6T14484C*.[36,46] However, biochemical data for the *ND6T14484C* mutation are conflicting. Normal respiration rate was also reported in cybrids derived from the EBV-transformed lymphoblasts. Meanwhile, reports on the effects of the mutant ND6 on complex I activity are controversial too. Normal complex I activity has been reported in fibroblasts,[41] platelets,[42] the lymphoblast cell line, and the lymphoblast-derived cybrids homoplasmic for *ND6T14484C*.[36] Meanwhile, decreased complex I activity has also been reported in the leukocytes of patients homoplasmic for the mutation, where complex I activity was reduced to about 40% of control values.[46] *In vivo* phosphorus (31P) magnetic resonance spectroscopy (p-MRS) studies showed that ND6T14484C induced a 47% decrease in the maximal rate of mitochondrial ATP synthesis in skeletal muscle; however, the reduction did not differ between the affected and unaffected subjects homoplasmic for the mutations.[47–49] These results suggest that other factors, in addition to ATP deficiency, influence the LHON phenotypic expression.

We found a pronounced increase in active CASPASE 3 expression in cells of the RGC layer in the mice injected with *hND6T14484C*. Similarly, Lin et al.[12] found an increase in complex I ROS production during forwarding electron flow in both liver and brain mitochondria of their ND6 P25L mice. In addition, Giordano et al.[50] found elevated ROS levels in an osteosarcoma-derived cybrid harboring the *ND6T14484C* mutation in galactose medium, and treatment with 7β-ostradiol led to the activation of the antioxidant enzyme superoxide dismutase and reduced apoptosis. In our data, the expression of antioxidant enzymes increased in the optic nerve at 1 month after the injection of mutant *hND6* when RGC did not lose function as detected using PERG. However, swelling of the optic nerve head and the adjacent RGC + IPL was found in these mice using SD-OCT. Ample evidence suggests that RGCs actively transport messenger RNAs into their axons and translate locally during the functional maintenance of the axons.[51–54] It is, therefore, reasonable to assume that mutant *hND6*-induced oxidative stress in the RGCs and their axons, as well as the elevated oxidative stress, eventually induced cell death in the retina. However, we cannot exclude RNA contamination from glial cells in the optic nerve. Further studies will be needed to use microdissected RGCs to address whether the elevated oxidative stress initiated in these cells.

In conclusion, we generated an LHON mouse model for the first time carrying *hND6T14484C*. The mice showed reductions in PERG amplitudes, progressive thinning of the RGC + IPL layers, and a loss of RGCs and their axon characteristics of human LHON. These mice will be an essential tool to study LHON pathogenesis and test potential treatments for the disease. We will use this model to test the therapeutic effects of MTS-AAV–delivered wild-type allele and then move on to stages of a trial. Future directions include generating a transgenic animal model by blastocyst injections of mutant *ND6,* as we have previously done for *ND4*. This work is needed because intravitreal injection of MTS-AAVs allows for delivery of the mutated gene of interest (*hND6T14484C*) only into the injected eye but not even into the contralateral eye. In contrast, blastocyst injection of MTS-AAVs delivers the mutated gene of interest to all tissues/organs. However, the load of interest gene varied between the tissues with the highest level in the RGCs and optic nerves.[27] Meanwhile, the RNA-seq data showed changes in many nuclear genes that will benefit us to explore the effects of impaired mitochondrial function on nuclear gene expression and identify new therapeutic targets for the disease.

Acknowledgments

Supported by R01s EY 017141 (JG) and EY 027414 (JG) and P30 EY014801 Bascom Palmer Eye Institute Core Grant (Vittorio Porciatti).

Disclosure: **H. Yu,** None; **D.W. Sant,** None; **G. Wang,** None; **J. Guy,** mito-targeted AAV (P)

References

1. Lopez Sanchez MI, Crowston JG, Mackey DA, Trounce IA. Emerging mitochondrial therapeutic targets in optic neuropathies. *Pharmacol Ther*. 2016;165:132–152.
2. Jurkute N, Yu-Wai-Man P. Leber hereditary optic neuropathy: bridging the translational gap. *Curr Opin Ophthalmol*. 2017;28:403–409.
3. Wallace DC, Singh G, Lott MT, et al. Mitochondrial DNA mutation associated with Leber's hereditary optic neuropathy. *Science*. 1988;242:1427–1430.

4. Yu-Wai-Man P, Griffiths PG, Chinnery PF. Mitochondrial optic neuropathies—disease mechanisms and therapeutic strategies. *Prog Retin Eye Res*. 2011;30:81–114.
5. Howell N, Bindoff LA, McCullough DA, et al. Leber hereditary optic neuropathy: identification of the same mitochondrial ND1 mutation in six pedigrees. *Am J Hum Genet*. 1991;49:939–950.
6. Huoponen K, Vilkki J, Aula P, Nikoskelainen EK, Savontaus ML. A new mtDNA mutation associated with Leber hereditary optic neuroretinopathy. *Am J Hum Genet*. 1991;48:1147–1153.
7. Johns DR, Neufeld MJ, Park RD. An ND-6 mitochondrial DNA mutation associated with Leber hereditary optic neuropathy. *Biochem Biophys Res Commun*. 1992;187:1551–1557.
8. Mackey D, Howell N. A variant of Leber hereditary optic neuropathy characterized by recovery of vision and by an unusual mitochondrial genetic etiology. *Am J Hum Genet*. 1992;51:1218–1228.
9. Spruijt L, Kolbach DN, de Coo RF, et al. Influence of mutation type on clinical expression of Leber hereditary optic neuropathy. *Am J Ophthalmol*. 2006;141:676–682.
10. Tonska K, Kodron A, Bartnik E. Genotype-phenotype correlations in Leber hereditary optic neuropathy. *Biochim Biophys Acta*. 2010;1797:1119–1123.
11. Yu-Wai-Man P, Griffiths PG, Brown DT, Howell N, Turnbull DM, Chinnery PF. The epidemiology of Leber hereditary optic neuropathy in the North East of England. *Am J Hum Genet*. 2003;72:333–339.
12. Lin CS, Sharpley MS, Fan W, et al. Mouse mtDNA mutant model of Leber hereditary optic neuropathy. *Proc Natl Acad Sci USA*. 2012;109:20065–20070.
13. Malfatti E, Bugiani M, Invernizzi F, et al. Novel mutations of ND genes in complex I deficiency associated with mitochondrial encephalopathy. *Brain*. 2007;130:1894–1904.
14. Koilkonda R, Yu H, Talla V, et al. LHON gene therapy vector prevents visual loss and optic neuropathy induced by G11778A mutant mitochondrial DNA: biodistribution and toxicology profile. *Invest Ophthalmol Vis Sci*. 2014;55:7739–7753.
15. Guy J, Qi X, Koilkonda RD, et al. Efficiency and safety of AAV-mediated gene delivery of the human ND4 complex I subunit in the mouse visual system. *Invest Ophthalmol Vis Sci*. 2009;50:4205–4214.
16. Qi X, Sun L, Lewin AS, Hauswirth WW, Guy J. The mutant human ND4 subunit of complex I induces optic neuropathy in the mouse. *Invest Ophthalmol Vis Sci*. 2007;48:1–10.
17. Ellouze S, Augustin S, Bouaita A, et al. Optimized allotopic expression of the human mitochondrial ND4 prevents blindness in a rat model of mitochondrial dysfunction. *Am J Hum Genet*. 2008;83:373–387.
18. Cwerman-Thibault H, Augustin S, Lechauve C, et al. Nuclear expression of mitochondrial ND4 leads to the protein assembling in complex I and prevents optic atrophy and visual loss. *Mol Ther Methods Clin Dev*. 2015;2:15003.
19. Cwerman-Thibault H, Augustin S, Ellouze S, Sahel JA, Corral-Debrinski M. Gene therapy for mitochondrial diseases: Leber hereditary optic neuropathy as the first candidate for a clinical trial. *C R Biol*. 2014;337:193–206.
20. Guy J, Feuer WJ, Davis JL, et al. Gene therapy for Leber hereditary optic neuropathy: low- and medium-dose visual results. *Ophthalmology*. 2017;124:1621–1634.
21. Feuer WJ, Schiffman JC, Davis JL, et al. Gene therapy for Leber hereditary optic neuropathy: initial results. *Ophthalmology*. 2016;123:558–570.
22. Koilkonda RD, Yu H, Chou TH, et al. Safety and effects of the vector for the Leber hereditary optic neuropathy gene therapy clinical trial. *JAMA Ophthalmol*. 2014;132:409–420.
23. Guy J, Feuer WJ, Porciatti V, et al. Retinal ganglion cell dysfunction in asymptomatic G11778A: Leber hereditary optic neuropathy. *Invest Ophthalmol Vis Sci*. 2014;55:841–848.
24. Koilkonda RD, Guy J. Leber's hereditary optic neuropathy-gene therapy: from benchtop to bedside. *J Ophthalmol*. 2011;2011:179412.
25. Yu H, Koilkonda RD, Chou TH, et al. Gene delivery to mitochondria by targeting modified adenoassociated virus suppresses Leber's hereditary optic neuropathy in a mouse model. *Proc Natl Acad Sci USA*. 2012;109:E1238–1247.
26. Yu H, Ozdemir SS, Koilkonda RD, et al. Mutant NADH dehydrogenase subunit 4 gene delivery to mitochondria by targeting sequence-modified adeno-associated virus induces visual loss and optic atrophy in mice. *Mol Vis*. 2012;18:1668–1683.
27. Yu H, Koilkonda RD, Chou TH, et al. Consequences of zygote injection and germline transfer of mutant human mitochondrial DNA in mice. *Proc Natl Acad Sci USA*. 2015;112:E5689–E5698.
28. Sant DW, Camarena V, Mustafi S, et al. Ascorbate suppresses VEGF expression in retinal pigment epithelial cells. *Invest Ophthalmol Vis Sci*. 2018;59:3608–3618.

29. Dobin A, Davis CA, Schlesinger F, et al. STAR: ultrafast universal RNA-seq aligner. *Bioinformatics*. 2013;29:15–21.
30. Love MI, Huber W, Anders S. Moderated estimation of fold change and dispersion for RNA-seq data with DESeq2. *Genome Biol*. 2014;15:550.
31. Porciatti V. The mouse pattern electroretinogram. *Doc Ophthalmol*. 2007;115:145–153.
32. Yang X, Chou TH, Ruggeri M, Porciatti V. A new mouse model of inducible, chronic retinal ganglion cell dysfunction not associated with cell death. *Invest Ophthalmol Vis Sci*. 2013;54:1898–1904.
33. Harvey AR, Kamphuis W, Eggers R, et al. Intravitreal injection of adeno-associated viral vectors results in the transduction of different types of retinal neurons in neonatal and adult rats: a comparison with lentiviral vectors. *Mol Cell Neurosci*. 2002;21:141–157.
34. Martin KR, Quigley HA, Zack DJ, et al. Gene therapy with brain-derived neurotrophic factor as a protection: retinal ganglion cells in a rat glaucoma model. *Invest Ophthalmol Vis Sci*. 2003;44:4357–4365.
35. Nickells RW, Schmitt HM, Maes ME, Schlamp CL. AAV2-mediated transduction of the mouse retina after optic nerve injury. *Invest Ophthalmol Vis Sci*. 2017;58:6091–6104.
36. Brown MD, Trounce IA, Jun AS, Allen JC, Wallace DC. Functional analysis of lymphoblast and cybrid mitochondria containing the 3460, 11778, or 14484 Leber's hereditary optic neuropathy mitochondrial DNA mutation. *J Biol Chem*. 2000;275:39831–39836.
37. Chen EY, Tan CM, Kou Y, et al. Enrichr: interactive and collaborative HTML5 gene list enrichment analysis tool. *BMC Bioinformatics*. 2013;14:128.
38. Kuleshov MV, Jones MR, Rouillard AD, et al. Enrichr: a comprehensive gene set enrichment analysis web server 2016 update. *Nucleic Acids Res*. 2016;44:W90–W97.
39. Subramanian A, Tamayo P, Mootha VK, et al. Gene set enrichment analysis: a knowledge-based approach for interpreting genome-wide expression profiles. *Proc Natl Acad Sci USA*. 2005;102:15545–15550.
40. Mootha VK, Lindgren CM, Eriksson KF, et al. PGC-1alpha-responsive genes involved in oxidative phosphorylation are coordinately downregulated in human diabetes. *Nat Genet*. 2003;34:267–273.
41. Cock HR, Cooper JM, Schapira AH. The 14484 ND6 mtDNA mutation in Leber hereditary optic neuropathy does not affect fibroblast complex I activity. *Am J Hum Genet*. 1995;57:1501–1502.
42. Carelli V, Ghelli A, Bucchi L, et al. Biochemical features of mtDNA 14484 (ND6/M64V) point mutation associated with Leber's hereditary optic neuropathy. *Ann Neurol*. 1999;45:320–328.
43. Hudson G, Carelli V, Spruijt L, et al. Clinical expression of Leber hereditary optic neuropathy is affected by the mitochondrial DNA-haplogroup background. *Am J Hum Genet*. 2007;81:228–233.
44. Chomyn A. Mitochondrial genetic control of assembly and function of complex I in mammalian cells. *J Bioenerg Biomembr*. 2001;33:251–257.
45. Bai Y, Attardi G. The mtDNA-encoded ND6 subunit of mitochondrial NADH dehydrogenase is essential for the assembly of the membrane arm and the respiratory function of the enzyme. *EMBO J*. 1998;17:4848–4858.
46. Oostra RJ, Van Galen MJ, Bolhuis PA, Bleeker-Wagemakers EM, Van den Bogert C. The mitochondrial DNA mutation ND6*14,484C associated with Leber hereditary optic neuropathy, leads to deficiency of complex I of the respiratory chain. *Biochem Biophys Res Commun*. 1995;215:1001–1005.
47. Lodi R, Taylor DJ, Tabrizi SJ, et al. In vivo skeletal muscle mitochondrial function in Leber's hereditary optic neuropathy assessed by 31P magnetic resonance spectroscopy. *Ann Neurol*. 1997;42:573–579.
48. Lodi R, Montagna P, Cortelli P, et al. 'Secondary' 4216/ND1 and 13708/ND5 Leber's hereditary optic neuropathy mitochondrial DNA mutations do not further impair in vivo mitochondrial oxidative metabolism when associated with the 11778/ND4 mitochondrial DNA mutation. *Brain*. 2000;123:1896–1902.
49. Barbiroli B, Montagna P, Cortelli P, et al. Defective brain and muscle energy metabolism shown by in vivo 31P magnetic resonance spectroscopy in nonaffected carriers of 11778 mtDNA mutation. *Neurology*. 1995;45:1364–1369.
50. Giordano C, Montopoli M, Perli E, et al. Oestrogens ameliorate mitochondrial dysfunction in Leber's hereditary optic neuropathy. *Brain*. 2011;134:220–234.
51. Gumy LF, Yeo GS, Tung YC, et al. Transcriptome analysis of embryonic and adult sensory axons reveals changes in mRNA repertoire localization. *RNA*. 2011;17:85–98.
52. Shigeoka T, Jung H, Jung J, et al. Dynamic axonal translation in developing and mature visual circuits. *Cell*. 2016;166:181–192.

53. Wong HH, Lin JQ, Strohl F, et al. RNA docking and local translation regulate site-specific axon remodeling in vivo. *Neuron*. 2017;95:852–868.e858.

54. Yoon BC, Jung H, Dwivedy A, O'Hare CM, Zivraj KH, Holt CE. Local translation of extranuclear lamin B promotes axon maintenance. *Cell*. 2012;148:752–764.